Available online at www.sciencedirect.com

ScienceDirect

Procedia CIRP 121 (2024) 204–209

www.elsevier.com/locate/procedia

11th CIRP Global Web Conference (CIRPe 2023)

# Structural aerospace component case study for additive friction stir deposition: Path planning, metrology, and CNC machining

Elijah Charles[a], Joshua Kincaid[a], Aaron Cornelius[a], Lauren Miller[a], Tony Schmitz[a,b,*]

[a]*Department of Mechanical, Aerospace, and Biomedical Engineering, University of Tennessee, Knoxville, 1512 Middle Drive, Knoxville, TN, 37996, USA*
[b]*Manufacturing Demonstration Facility, Oak Ridge National Laboratory, 2350 Cherehala Blvd, Knoxville, TN, 37932, USA*

*Corresponding author. Tel.: +1-865-974-6141; E-mail address: tony.schmitz@utk.edu

**Abstract**

A common aerospace and defense industry challenge is low volume production of components for legacy aircraft due to compromised casting and forging supply chains. A hybrid manufacturing approach is presented to address this challenge that uses additive friction stir deposition, structured light scanning, and CNC milling. The paper describes a novel slicing and toolpath development strategy for additive friction stir deposition of a relevant aerospace geometry, post deposition measurement of the two-sided preform and identification of the machining work coordinate system, and five-axis CNC machining to obtain the final part geometry while ensuring stable machining behavior.



*Keywords:* Hybrid manufacturing, additive friction stir deposition, structured light scanning, milling

## 1. Introduction

The combined use of additive manufacturing (AM) and subtractive manufacturing (SM), or machining, methods in integrated workflows, or hybrid manufacturing, offers several benefits not available when using the two separately, including: 1) increased part complexity coupled with dimensional accuracy and surface finish [1]; and 2) the timely and cost-effective manufacture of components for which low volume production is needed and tooling is scarce, no longer exists, or is damaged beyond usefulness [2]. In the aerospace industry, increasing difficulty in domestic sourcing of 7000-series aluminum castings and forgings is a national security concern, especially for military modified aircraft requiring spare components past their production phase. Production of new tooling for these parts is not economically viable due to the low volume of spares needed to keep the aircraft functional and the lack of suppliers willing to produce castings and forgings at such a reduced scale. However, for hybrid manufacturing to address the casting and forging spare part supply chain issues, AM techniques must enable scale up and reliable performance. For components originating from additive processes, robust toolpath generation software is required to enable mainstream adoption and deployment of the hybrid manufacturing strategy.

Additive friction stir deposition (AFSD) is a solid-state AM process showing promising capability to enable the hybrid manufacturing of aluminum aerospace parts. Current efforts are focused on the ability to produce parts for multiple industries at the meter scale and larger. Applications include part repair [3] and preform production as an alternative for parts with short timelines, castings, forgings, and spare parts [4]. AFSD enables fully dense consolidation of materials that is difficult or impractical to replicate using fusion-based welding processes, for example, and controllable microstructure and properties variation via process parameter adjustment and in-situ control [5].

It has previously been established that AFSD provides a solid-state alternative to beam-based AM [6-9], where the

2212-8271 
10.1016/j.procir.2023.08.065

feed material is not melted. Instead, the preform geometry and microstructure are defined by the AFSD process kinetic energy. Related search efforts have studied the important property-parameter-microstructure relationships [10-19].

The AFSD process applied here accomplishes solid-state metal alloy deposition through the extrusion and shear-induced plastic deformation of a square cross-section bar of the desired material. This is done at a prescribed material feed rate (MFR). A tool-spindle assembly containing a square bore constrains the feedstock as it is fed and stirred onto a substrate material. Spindle rotation provides heat generation through contact friction between the tool shoulder and deposited metal, as well as through internal shear deformation mechanisms. Deposition is made possible through the lateral movement of the tool at a prescribed tool feed rate (TFR), which indicates the tool velocity along the prescribed motion path; similar to machining operations, it can be described as the feed per revolution multiplied by the spindle rotation speed, Ω. The feed-rotation kinematics enable tracks with high width-to-thickness ratios to be bonded to the substrate and previous layers. See Fig. 1.

**Nomenclature**

| | |
|---|---|
| AFSD | additive friction stir deposition |
| MFR | material feed rate |
| TFR | tool feed rate |
| FRF | frequency response function |

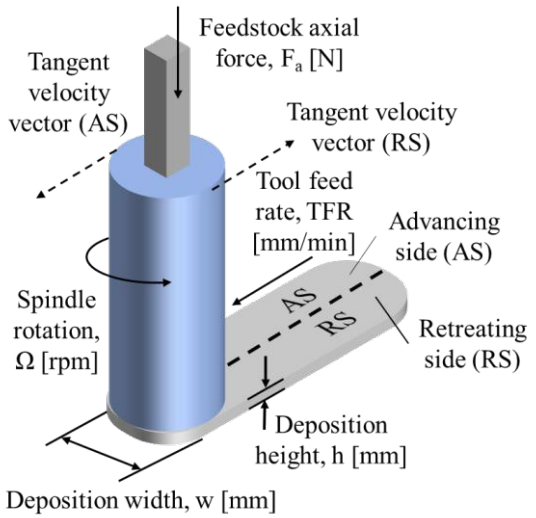


Fig. 1. Diagram of the AFSD process.

While AFSD has been demonstrated as a capable metal additive technology, little work has been done on hybrid strategies for large-scale component fabrication. Contrary to AM processes characterized by high resolution and small layer size relative to the part volume, AFSD requires specialized path planning due to track overlaps and the associated process transients. Additionally, MFR and TFR must be actively adjusted along a toolpath to compensate for these overlaps and maintain a homogenous deposit. This work provides a case study to demonstrate AFSD path planning and key considerations for a relevant aerospace part geometry; see Fig. 2.

The remainder of this paper presents: 1) toolpath shell modelling used in conjunction with open-source slicing software; and 2) toolpath coordinate modification and machine code production as an approach to generating AFSD toolpaths for non-uniform geometries. An analysis of the AFSD preform thermal history is also provided as both spatial and section-segregated distributions to provide insight into the influence of the toolpath on the process behavior. Descriptions of the preform measurement using structured light scanning, the use of the scanned model for machining path planning, and machining considerations, including fixturing design and part tap testing, are also provided.

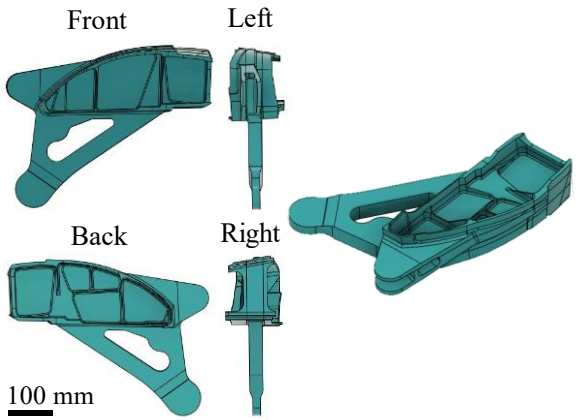


Fig. 2. Aerospace part geometry selected for the case study.

## 2. AFSD

As illustrated in Fig. 3, efforts for the additive component began with the part geometry and a deposition strategy. It was decided to use plate stock for the midline portion of the part with deposition on both sides of the 609.6 mm by 609.6 mm by 38.1 mm 7075 aluminum plate. The part orientation relative to the plate was selected to capture as much solid mid-section geometry as possible.

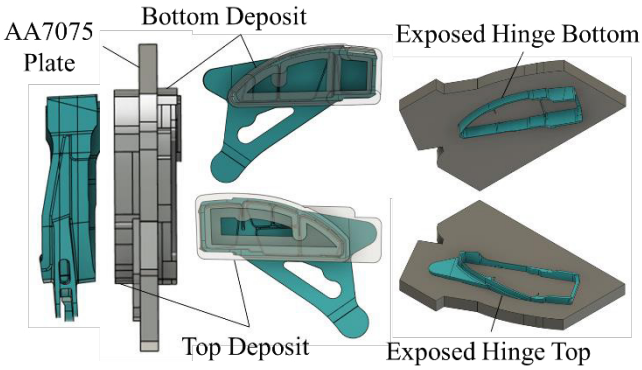


Fig. 3. Relative orientation of plate and part chosen to enable two-sided deposition strategy, leaving thin wall features exposed.

Waterjet and dovetail machining were performed prior to AFSD to remove excess material around the preform's boundary and provide work holding features for the final five-axis milling operations; see Fig. 4. The two-sided deposition strategy required deposition on one face, followed by a facing operation to make that surface flat. This flat surface served as the base for deposition on the other face.

A CAD-based approach was implemented for the AFSD toolpath planning. This was motivated by the varying cross-

sectional shape of the outer contour and rib geometry throughout the build direction of the front and back surface depositions. The CAD-based modeling included horizontally sectioned toolpath shells in the absence of dedicated toolpath generation software. The part width near the plate (lower section on the first, or top, side) required track overlap and two parallel toolpaths. The upper section further from the plate surface included the outer thin-wall contour so a helix-based closed-loop toolpath was selected. The top side deposition toolpath sections are shown in Fig. 5.

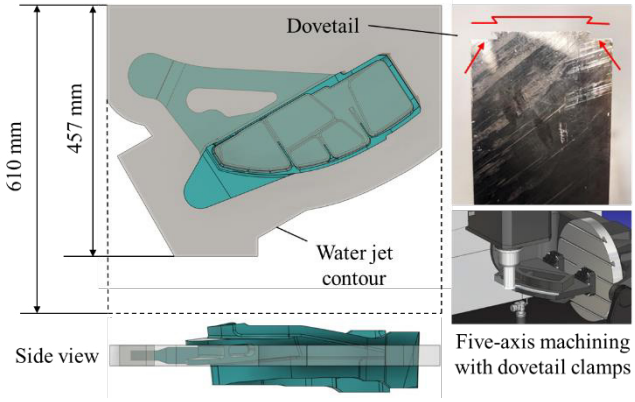


Fig. 4. Excess material removal by water jet and dovetail for work holding during five-axis machining.

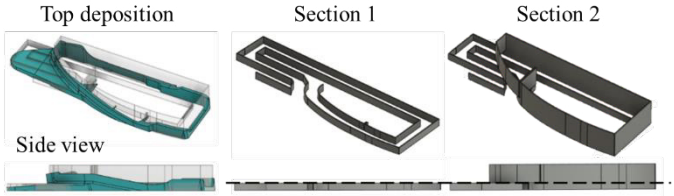


Figure 5: Part top deposition; the lower section 1 containing localized, solid geometry and appropriate overlaps and the upper section 2 containing remaining outer part contours are also shown.

The second, or bottom, side deposition was split into three toolpath sections; see Fig. 6. An open-loop toolpath was selected that alternated deposition direction with each layer and section. This approach was chosen because a closed-loop toolpath was difficult to implement given the rib geometry which spanned the entire part. The open-loop strategy allowed the tool to make layer changes locally within layers at natural toolpath ends. After the toolpath shells were defined, they were converted to an STL file format required for use in an open-source slicer suite. Prusa Research's PrusaSlicer 2.5.0 was selected for this research. The unrefined toolpath trajectories are shown in Fig 7.

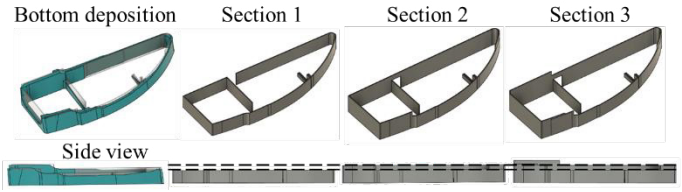


Figure 6: Part bottom deposition; the lower section 1, middle section 2, and upper section 3 are also shown.

Machine code development in MATLAB followed CAD modeling and slicing of the toolpath shells as the final step before AFSD could be performed. Programmed regular expression identifiers were used to select text strings in the unrefined G-code files generated for both sliced toolpath shells and sequentially extract and tabulate X and Y coordinates into arrays. Points were then separated into sub-arrays by deposition section, after which each section required unique coding logic to develop the desired toolpath; see Fig. 8. Conditioning steps were completed for each section's sub-array of coordinate data. These steps were: point-spacing homogenization, assignment of modified Z-coordinates and toolpath directions, assignment of adjusted MFR values if track overlapping existed, and calculation of feedstock depletion locations needed to indicate to the machine when a reload cycle was necessary (for the MELD Manufacturing L3 machine used in this study, a discrete feed approach is used where each wrought bar is 508 mm long). See Figs. 9 and 10.

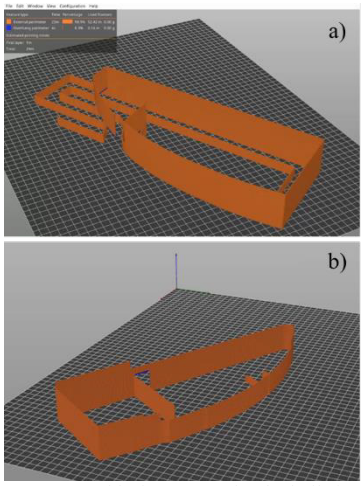


Figure 7: a) The part top and b) bottom toolpath shells in the PrusaSlicer user interface. Each section was given a work coordinate system origin at the plate's corner.

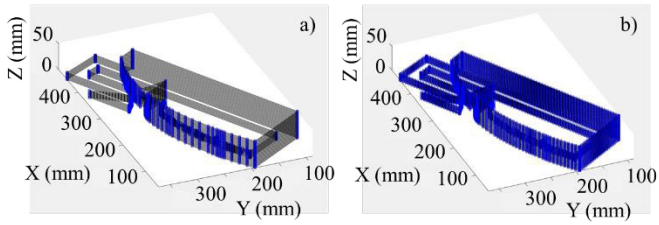


Figure 8: a) Example of toolpath points with variable spacing generated by PrusaSlicer software and b) modification of point spacing by adding points between original toolpath points with uniform spacing.

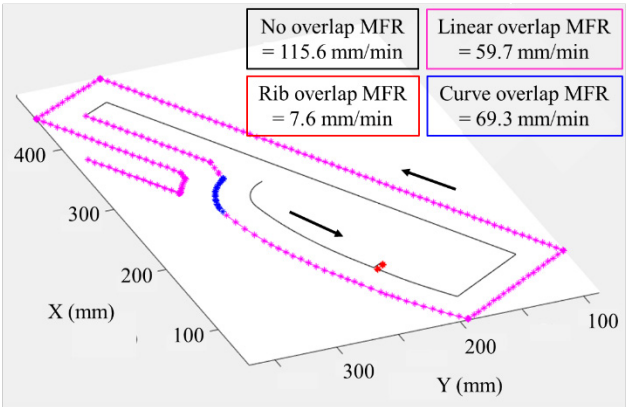


Figure 9: Layer from top side first section showing adjusted MFRs along overlap locations. Red asterisks identify overlaps containing rib geometry, while magenta and blue asterisks identify linear and curve overlaps.

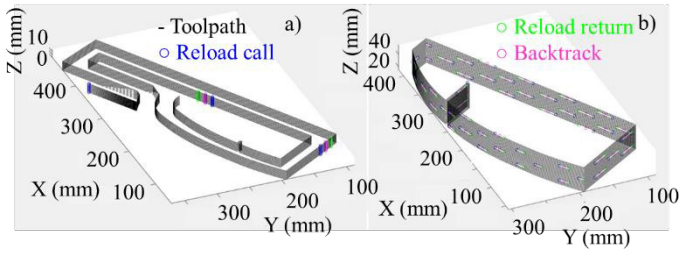


Figure 10: Identification of deposition stop locations in blue, tool return positions for deposition restart in green, and tool location for reprocessing of previously finished deposition tracks following deposition restart in magenta. a) Top, b) bottom.

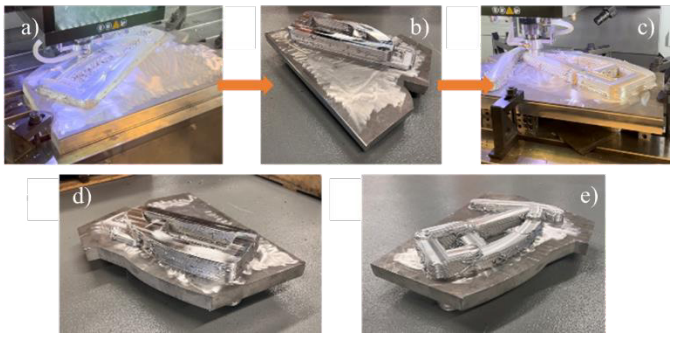


Figure 11: a) Deposition of the top side preform, b) facing the top side preform to provide a flat, 50.8 mm-tall surface for support during bottom side deposition, c) deposition of the bottom side, d) completed top side preform, and e) completed bottom side preform.

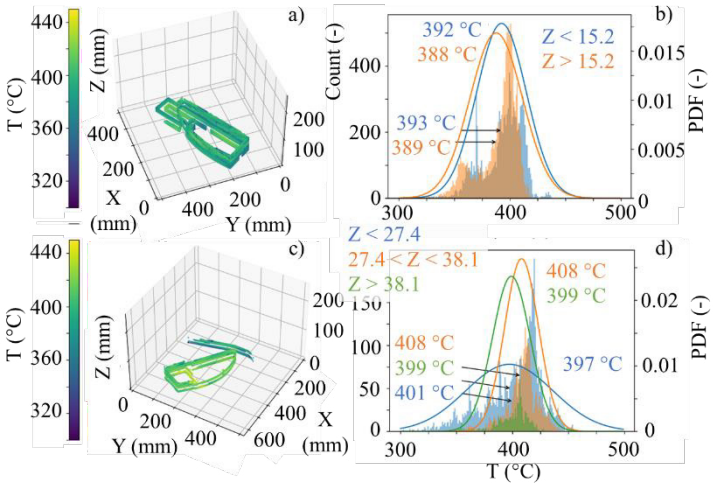


Figure 12: a) Spatial temperature variation for the top side, b) temperature histograms for the first (orange) and second (blue) toolpath sections, c) spatial temperature variation for the bottom side, and d) histograms for the first (blue), second (orange), and third (green) sections.

The deposition sequence is displayed in Fig. 11. The top side was deposited on the plate first. The top surface of this deposition was then machined flat. The part was then flipped so that the flat top surface served as the base for the bottom side deposition. Temperature data was collected during deposition using a tool-embedded thermocouple. This enabled visualization of thermal cycles and temperature distribution throughout both deposition sides (see Fig. 12). Observations include the slight variation of mean and median temperature with each toolpath section, as well as the elevation of steady state temperature above the selected processing set point of 350 °C. This indicates heat build-up in the part during deposition as well as a small increase in the initially selected lower spindle speed limit from 70 rpm to 95 rpm due to insufficient material yielding at the lower limit. Repeated passes over a selected spatial location explains the increased mean and median temperatures, including toolpaths on the top side deposition's first section, in which overlapping provided more processing cycles at localized regions of the build per layer.

## 3. Metrology

The preform was scanned using a GOM ATOS Q structured light scanner to create a 3D model of the as-printed geometry. In prior work using structured light scanning to inspect additive preforms before machining, the scan has been aligned to the nominal as-machined CAD model with a least-squares best fit to determine the optimal CAD/print alignment for machining [6]. However, for this part the nominal model was significantly different than the print due to the large bead width. Therefore, the scan was instead aligned to a separate CAD model depicting the expected print geometry (see Fig. 13). As shown, the walls were wider than expected by roughly 16 mm and shorter by 2 mm. Overall, however, there was sufficient extra material to ensure that the part was fully contained within the preform.

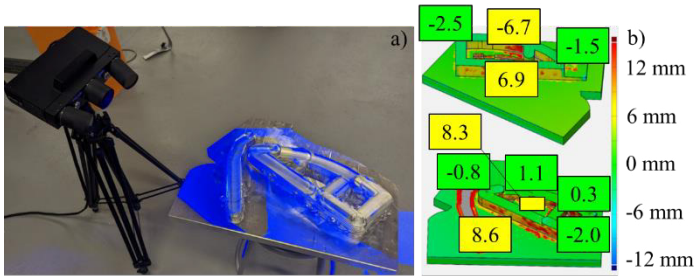


Figure 13: a) Scanning the part with the structured light scanner. b) Scanned part compared to the expected print geometry. The color bar shows the surface deviation compared to the CAD model.

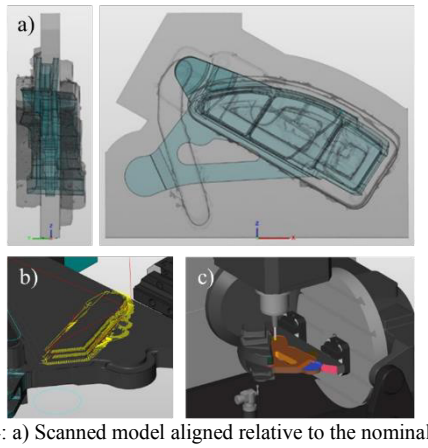


Figure 14: a) Scanned model aligned relative to the nominal CAD in Hypermill, b) optimized machining toolpaths based on the scanned stock model, and c) part machining simulation for collision detection and program verification using the preform scan as a stock model.

The scanned model was then reduced in resolution, made watertight, and imported into the Hypermill CAM software to program the machining toolpaths using the strategies described in [6]. Since the expected print model was constructed in the same coordinate system as the nominal CAD model, the imported scan was already aligned

to the part geometry as shown in Fig. 14. The toolpaths were then optimized using the scan as the stock model to add cutting passes in areas where more material was present than expected and reduce cycle time by removing non-cutting air-passes. The scan was also used for collision detection and machining simulation to validate the machining program. The differences between the modeled and physical preform (Fig. 13) are based on nominal CAD modeling using 38.1 mm track widths. Because the intent was to use the preform scan as the CAM stock model, the CAD model was only intended to provide an approximate digital representation of the preform.

## 4. Machining

The preform was machined using a Haas UMC-1000 five-axis CNC machining center. The part was constrained vertically using dovetail vises, which clamped onto a 2 mm dovetail machined on the edge of the plate used for two-sided deposition; see Fig. 15. While this orientation did not provide maximum part stiffness (due to the cantilever orientation), it did provide access to all part features in a single machining operation without required specialized fixturing. Note that the dovetail was machined prior to printing since the added material would have made it difficult to fixture the preform to cut the dovetail (see Fig. 4). Additional clamps were used during the final operation, where the part was removed from the remaining plate.

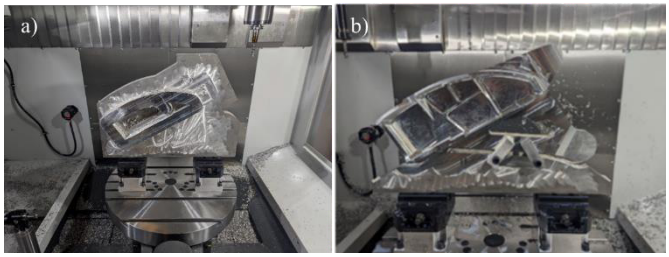


Figure 15: a) Preform clamped on the five-axis machine tool before machining. b) Additional clamps secured the part during cut-off.

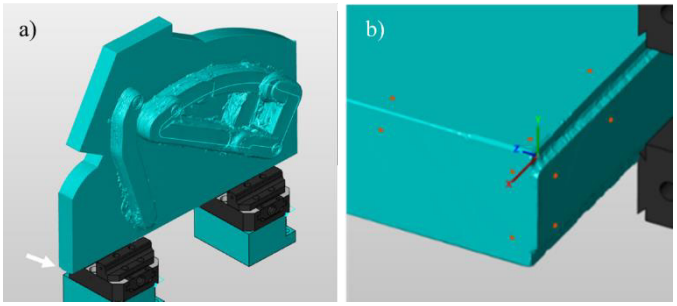


Figure 16: a) The corner of the part was probed to establish the coordinate system and b) closeup of the probing points (orange) and the reconstructed machine tool coordinate system used in Hypermill.

The machine tool's work coordinate offset was set using the scanned model of the preform; see Fig. 16. Previous work implemented this approach by attaching a set of fiducials to the preform, scanning the assembly, and probing those fiducials on the machine tool [20-21]. Here, the corner of the part was used as a fiducial. Since the corners of the build plate had not been machined perpendicular to each other, three points were probed on each side of the corner. These nine probed points defined three planes which were used to kinematically reconstruct the machine tool coordinate system inside of Hypermill. The cutting toolpaths were then regenerated based on this new coordinate system to compensate for the actual position and orientation of the part on the machine tool. Because of this compensation, the part did not need to be manually aligned with the machine axes.

The preform's frequency response function, FRF, was measured by modal, or tap, testing to verify that the fixturing setup was stiff enough for machining [22]. Figure 17 shows the direct frequency response function measured at the tip of the preform. The dominant mode had a 53 Hz natural frequency, which was significantly below the tooth passing frequencies for combinations of spindle speed and the cutting tools used during machining. For example, the three tooth, 12.7 mm diameter endmill used for most of the roughing had a tooth passing frequency of 405 Hz at 8100 rpm. As a result, the 53 Hz mode was not excited and had little impact on machining. The part was fully machined without encountering chatter.

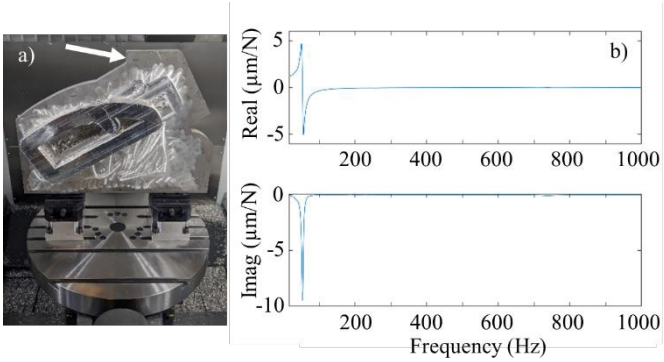


Figure 17: a) Tap testing location at the tip of the part. b) Direct FRF measured by tap testing with 53 Hz bending mode.

Figure 18: Photographs of fully machined component.

## 5. Conclusions and outlook

This paper described the fabrication of an aerospace component using AFSD, structured light scanning, and five-axis machining. Results were presented for toolpath shell modelling using an open-source slicing software; toolpath coordinate modification and machine code production for AFSD with non-uniform geometries; in-process temperatures to visualize the thermal history; preform measurement using structured light scanning; the use of the scanned model for machining path planning; and machining considerations, including fixturing design and part tap testing. The 7075 aluminum deposition proceeded as planned and no major issues were encountered during machining. The finished part shown in Fig. 18 required 18.2 hrs of AFSD time and 19 hrs of machining time. The AFSD process time was extended by the manual bar loading, which averaged 3

min/bar (actual deposition time was 11.9 hrs). The machining time was limited by: 1) conservative machining parameters were selected out of concern for the structural integrity of the dovetail; and 2) the machine tool had a maximum spindle speed of 8100 rpm, which is low for traditional aluminum milling.

## Acknowledgements

Support was provided by DEVCOM Army Research Laboratory under grant no. W911NF2120020. The authors also thank Drs. P. Metz and S. Babu, University of Tennessee, Knoxville, for the thermal analysis and Dan Braley, The Boeing Company, for the part design.

## References

[1] Korkmaz, M.E., Waqar, S., Garcia-Collado, A., Gupta, M.K. and Krolczyk, G.M., 2022. A technical overview of metallic parts in hybrid additive manufacturing industry. Journal of Materials Research and Technology.

[2] Mellor, S., Hao, L. and Zhang, D., 2014. Additive manufacturing: A framework for implementation. International journal of production economics, 149, pp.194-201.

[3] Peter Martin, L., Luccitti, A. and Walluk, M., 2022. Evaluation of additive friction stir deposition for the repair of cast Al-1.4 Si-1.1 Cu-1.5 Mg-2.1 Zn. Journal of Manufacturing Science and Engineering, 144(6).

[4] Hang, Z.Y., 2022. Additive Friction Stir Deposition. Elsevier.

[5] Mishra, R.S., Haridas, R.S. and Agrawal, P., 2022. Friction stir-based additive manufacturing. Science and Technology of Welding and Joining, 27(3), pp.141-165.

[6] Hang, Z.Y., Jones, M.E., Brady, G.W., Griffiths, R.J., Garcia, D., Rauch, H.A., Cox, C.D. and Hardwick, N., 2018. Non-beam-based metal additive manufacturing enabled by additive friction stir deposition. Scripta Materialia, 153, pp.122-130.

[7] Khodabakhshi, F. and Gerlich, A.P., 2018. Potentials and strategies of solid-state additive friction-stir manufacturing technology: A critical review. Journal of Manufacturing Processes, 36, pp.77-92.

[8] Yu, H.Z. and Mishra, R.S., 2021. Additive friction stir deposition: a deformation processing route to metal additive manufacturing. Materials Research Letters, 9(2), pp.71-83.

[9] Gopan, V., Wins, K.L.D. and Surendran, A., 2021. Innovative potential of additive friction stir deposition among current laser based metal additive manufacturing processes: A review. CIRP Journal of Manufacturing Science and Technology, 32, pp.228-248.

[10] Priedeman, J.L., Phillips, B.J., Lopez, J.J., Tucker Roper, B.E., Hornbuckle, B.C., Darling, K.A., Jordon, J.B., Allison, P.G. and Thompson, G.B., 2020. Microstructure development in additive friction stir-deposited Cu. Metals, 10(11), p.1538.

[11] Perry, M.E., Griffiths, R.J., Garcia, D., Sietins, J.M., Zhu, Y. and Hang, Z.Y., 2020. Morphological and microstructural investigation of the non-planar interface formed in solid-state metal additive manufacturing by additive friction stir deposition. Additive Manufacturing, 35, p.101293.

[12] Griffiths, R.J., Garcia, D., Song, J., Vasudevan, V.K., Steiner, M.A., Cai, W. and Hang, Z.Y., 2021. Solid-state additive manufacturing of aluminum and copper using additive friction stir deposition: Process-microstructure linkages. Materialia, 15, p.100967.

[13] Agrawal, P., Haridas, R.S., Yadav, S., Thapliyal, S., Gaddam, S., Verma, R. and Mishra, R.S., 2021. Processing-structure-property correlation in additive friction stir deposited Ti-6Al-4V alloy from recycled metal chips. Additive Manufacturing, 47, p.102259.

[14] Phillips, B.J., Mason, C.J.T., Beck, S.C., Avery, D.Z., Doherty, K.J., Allison, P.G. and Jordon, J.B., 2021. Effect of parallel deposition path and interface material flow on resulting microstructure and tensile behavior of Al-Mg-Si alloy fabricated by additive friction stir deposition. Journal of Materials Processing Technology, 295, p.117169.

[15] Perry, M.E., Rauch, H.A., Griffiths, R.J., Garcia, D., Sietins, J.M., Zhu, Y., Zhu, Y. and Hang, Z.Y., 2021. Tracing plastic deformation path and concurrent grain refinement during additive friction stir deposition. Materialia, 18, p.101159.

[16] Williams, M.B., Robinson, T.W., Williamson, C.J., Kinser, R.P., Ashmore, N.A., Allison, P.G. and Jordon, J.B., 2021. Elucidating the effect of additive friction stir deposition on the resulting microstructure and mechanical properties of magnesium alloy we43. Metals, 11(11), p.1739.

[17] Mukhopadhyay, A. and Saha, P., 2022. A critical review on process metrics–microstructural evolution–process performance correlation in additive friction stir deposition (AFS-D). Journal of the Brazilian Society of Mechanical Sciences and Engineering, 44(9), p.422.

[18] Joshi, S.S., Sharma, S., Radhakrishnan, M., Pantawane, M.V., Patil, S.M., Jin, Y., Yang, T., Riley, D.A., Banerjee, R. and Dahotre, N.B., 2022. A multi modal approach to microstructure evolution and mechanical response of additive friction stir deposited AZ31B Mg alloy. Scientific Reports, 12(1), p.13234.

[19] Zeng, C., Ghadimi, H., Ding, H., Nemati, S., Garbie, A., Raush, J. and Guo, S., 2022. Microstructure evolution of Al6061 alloy made by additive friction stir deposition. Materials, 15(10), p.3676.

[20] Cornelius, A., Dvorak, J., Jacobs, L., Penney, J. and Schmitz, T., 2021. Combination of structured light scanning and external fiducials for coordinate system transfer in hybrid manufacturing. Journal of Manufacturing Processes, 68, pp.1824-1836.

[21] Dvorak, J., Cornelius, A., Corson, G., Zameroski, R., Jacobs, L., Penney, J. and Schmitz, T., 2022. A machining digital twin for hybrid manufacturing. Manufacturing Letters, 33 (Supplement).

[22] Schmitz, T. and Smith, K.S., Machining Dynamics: Frequency Response to Improved Productivity (2009). Springer.